Final Draft
of the original manuscript:

Yasakau, K.A.; Kuznetsova, A.; Kallip, S.; Starykevich, M.; Tedim, J.; Ferreira, M.G.S.; Zheludkevich, M.L.:

A novel bilayer system comprising LDH conversion layer and sol-gel coating for active corrosion protection of AA2024.

In: Corrosion Science. Vol. 143 (2018) 299 - 313.
First published online by Elsevier: August 20, 2018

DOI: /10.1016/j.corsci.2018.08.039
https://dx.doi.org/10.1016/j.corsci.2018.08.039

A novel bilayer system comprising LDH conversion layer and sol-gel coating for active corrosion protection of AA2024

K.A. Yasakau[1*], A. Kuznetsova[1], S. Kallip[1,2], M. Starykevich[1], J. Tedim[1], M.G.S. Ferreira[1], M.L. Zheludkevich[1,3]

[1] Department of Materials and Ceramic Engineering, CICECO - Aveiro institute of materials, University of Aveiro, 3810-193 Aveiro, Portugal.
[2] Institute of Chemistry, University of Tartu, Ravila 14a 50411, Tartu, Estonia.
[3] MagIC – Magnesium Innovation Centre, Institute of Materials Research Helmholtz-Zentrum Geesthacht, Max-Planck Str. 1, 21502 Geesthacht, Germany.

Abstract

In this work active corrosion protection of AA2024 by a bilayer system consisting of a LDH (layered double hydroxides) conversion layer coated by a sol-gel film was studied. Impedance and Scanning vibrating electrode technique (SVET) studies demonstrated an efficient active corrosion protection and self-healing abilities of the systems containing LDH layer loaded with vanadate corrosion inhibitor. Microstructural and chemical analysis of the surface after corrosion testing showed accumulation of chlorine signal in LDH coatings. The scavenging of chlorides and release of vanadate inhibitor from LDH layer can explain high efficiency of corrosion inhibition of AA2024 by the novel protective system.

Keywords: Active corrosion protection; Layered double hydroxides; Sol-gel coatings; vanadate inhibitor; self-healing.

[*] Corresponding author: K.A. Yasakau, Department of Materials and Ceramic Engineering, CICECO, University of Aveiro, 3810-193 Aveiro, Portugal, Tel.: +351-234-401418; Fax: +351-234-378146
E-mail address: kyasakau@ua.pt

1. **Introduction**

The uncontrolled corrosion damage of structural parts of airplanes may cause mechanical failures leading to disastrous accidents. Complex multilayer corrosion protective systems are commonly used for corrosion protection of metallic parts prone to corrosion damage such as aluminium alloys which are relevant materials for aerospace applications. State of the art corrosion protective systems in aerospace industry are comprised of a top coat, primer and pre-treatment [1]. In spite of improved protection characteristics of the coatings, the industry is burdened with expensive revisions, maintenance procedures and repainting/replacement of the damaged parts due to lacking the means for monitoring the extent of corrosion damage under the coated parts. Therefore the efforts have been placed on how to improve the multi-layer corrosion protective systems and achieve better active corrosion protection functionalities able to prolong corrosion protection of aluminium alloys.

Each of the layers in a corrosion protective scheme has its own functionality. For example, a tough top coat provides a barrier against the environment, UV radiation and mechanical impacts. More intricate role is provided by a primer and pre-treatment. A primer is responsible for storage and release of corrosion inhibitive additives such as the state of the art Cr (VI) pigments and others inorganic pigments [2]. Unfortunately, due to health risks of chromates its application in industry became very limited and will be abandoned in future. Much of research was concentrated on finding Cr-free solutions and developing containers for storage and release of corrosion inhibitors. Several groups have developed reservoirs of inhibitors to be combined with different primers based on layered double hydroxides (LDH) [3-6]. LDH compounds loaded with decavanadate, vanadate, phosphate, and 2-mercaptobenzothiazolate showed promising results in active corrosion protection of AA2024. Pigments based on rare earth organophosphate compounds [7, 8] and polyelectrolyte capsules of inhibitor [9, 10] have been used as additives to organic primers, which provide efficient corrosion protection of aluminium alloys.

An additional corrosion protection of aluminium alloys may be achieved by a proper surface pre-treatment which integrates inhibiting species within. However, one of the major benefits of such pre-treatments is enhanced interface adhesion between a metal and organic coatings. Traditionally chromate based pre-treatments have been used, which demonstrate efficient corrosion protection and adhesion [11]. In order to cope with the environmental regulations different Cr-free conversion coatings have been developed with several alternatives on the table such as anodic films [1, 12], conversion coatings [13-15], inorganic hydrotalcite

coatings [16]. Corrosion inhibition functionality of such coatings depends on whether the coating contains inhibiting ions efficient in corrosion protection of the underlying aluminium alloys. Thin pre-treatments have limited capacity to incorporate inhibitive species needless to say containers of inhibitors. Unless a pre-treatment has intrinsic inhibitive properties e.g. cerate, chromate type, there are a few alternatives such as porous anodic layers, mixed hydroxide layers (LDH) and sol-gel coatings which can successfully include inhibitors. In the case of anodic films sealing of the pores with LDH has been used to enhance active corrosion protection of the films [17, 18]. LDH is able to store and release inhibitive vanadate anions providing efficient corrosion protection of AA2024 [17]. More recently LDH conversion films have been directly grown on the surface of AA2024 [19]. These LDH films have defined anionic exchange abilities making them good storage units for anionic inhibitors unlike hydrotalcite ones having intercalated carbonate species which are not prone to anionic exchange. Anionic species in LDH films were substituted for inhibiting vanandates anions thus conferring active corrosion protection functionality to the films.

Contrary to anodic films and inorganic conversion coatings hybrid sol-gel pre-treatments combine inorganic and organic properties and effectively improve adhesion towards both metal and organic paints [20]. Admittedly a simple unmodified sol-gel matrix is not capable to provide active corrosion protection. This calls for a substantial improvement of the coatings by introducing various corrosion inhibitors either as inorganic [21-23] or organic [24, 25]. However, a simple addition of inhibitors to a sol-gel matrix cannot be attractive due to possible interactions between inhibitors and sol-gel, uncontrollable release of inhibitors and loss of barrier properties. To overcome these problems various inhibitor containers and nano-scale additives have been developed to impart active corrosion protection functionality on sol-gel systems [26-28]. The literature offers little information regarding the corrosion protection efficiency of sol-gel coatings loaded with LDH containers [5, 29]. Although containers of inhibitors generally enhance the corrosion protective properties of sol-gel coatings, the maximum amount of the containers that a coating can accommodate is low.

The inhibitor loading can be increased by successfully combining two surface treatment approaches such as a LDH conversion layer and a sol-gel coating. The double layer system may provide additional benefits such as uniform distribution of the LDH containers over the metal surface and an improved delivery rate of the inhibitor located very close to the metal surface. Moreover, the hybrid layer on top of LDH-conversion coating can be used as an effective primer insuring reasonable barrier properties and, more importantly, good adhesion to both the LDH

layer and a polymer top coat. However, such LDH pre-treatments in combination with hybrid sol-gel coatings have not been thoroughly studied yet. Moreover, there is a lack of information regarding surface uniformity, compatibility with hybrid/organic coatings and active corrosion protection (self-healing) efficiency in a multilayer scheme.

Therefore, the aim of this work was to investigate synergy between a LDH pre-treatment and hybrid sol-gel matrix acting as a Cr (VI) free corrosion protective system for AA2024. This work has explored several steps which might affect the efficiency of corrosion protection by the bilayer pre-treatment. Particularly, the attention has been given to the surface cleaning process of AA2024, the type of the incorporated anions in the LDH structure and the presence of a sol-gel film. The main techniques for investigation of corrosion protection effectiveness were Electrochemical Impedance Spectroscopy (EIS) and Scanning Vibrating Electrode Technique (SVET). The microstructure and chemical properties of the coatings were explored by electron microscopy, and spectroscopy methods.

2. Experimental

2.1 Materials

Aluminium alloy AA2024-T3 containing the following alloying elements (wt.%): Cu 3.8–4.9; Fe 0.5; Cr 0.1; Mg 1.2–1.8; Mn 0.3–0.9; Si 0.5; Ti 0.15; Zn 0.25; other 0.15 was used in this study. Aluminium coupons with dimensions 3× 4.5× 0.1 cm were chemically cleaned according to two procedures (Table 1). The first pre-treatment procedure (#1) consisted of the alloy cleaning at room temperature during 120 s in dilute 0.1 M NaOH (CAS 1310-73-2 Sigma-Aldrich) solution. Then, the plates were etched during 480 s in a 0.1 M HNO_3 (CAS 7697-37-2 Alfa Aesar) solution. Each step was followed by washing with deionised water. Finally, the AA2024 plates were sonicated in ethanol for 5 minutes and dried in air. The samples pre-treated according to this procedure were denominated as #1 (Table 1). The second procedure (#2) consisted of cleaning in Metaclean T2001 (based on alkaline metal silicates with complexing, and surface active agents) at about 65 °C during 25 min followed by rinsing with deionized water. CFGAfterwards the specimens were etched in Turco™ Liquid Aluminetch N2 (based on sodium hydroxide and phosphates) at 65 °C during 45 sec and rinsing with deionized water and acid etching in Turco™ Liquid Smutgo NC (based on Ferric Sulfate, Nitric Acid, Sodium Hydrogendifluoride, Sulfuric Acid) at 30 °C during about 5 min followed by rinsing with deionized water and drying in air. The samples pre-treated according to this procedure were denominated as #2 (Table 1).

2.2 LDH and Sol-gel synthesis.

LDH synthesis

The LDHs conversion layer was synthesized as described in previous works [19]. Aluminium alloy substrates were immersed in a 5 mM zinc nitrate (CAS 10196-18-6 Sigma-Aldrich) solution (pH adjusted to 7) for a few hours at 100ºC. The substrates were then removed from solution, washed and dried. At this point, LDH(NO3) films had been formed on the metal surface. Afterwards, the plates were immersed in a second solution of 0.1 M $NaVO_3$ (CAS 13718-26-8 Sigma-Aldrich) (pH 8-9) for a couple of hours at 50ºC. The plates were finally washed with ultrapure water, ethanol (>98%), and then dried in air. After this process, AA2024 plates with LDH films intercalated with vanadates were obtained LDH(V2O7).

The LDH(V2O7) powder for inhibitor release studies was synthesized by anion-exchange using LDH(NO3) as a pristine LDH, the latter was prepared by co-precipitation route according to the procedure described in detail in [4].

Sol-gel synthesis

Hybrid sols were prepared by a controllable hydrolysis of zirconium (IV) propoxide (TPOZ) (CAS 23519-77-9 Alfa Aesar) and 3- glycidoxypropyltrimethoxysilane (GPTMS) (CAS 2530-83-8 Alfa Aesar) precursors in 2-propanol (CAS 67-63-0 Sigma-Aldrich). At first TPOZ (70 wt.% in 2-propanol) was mixed with ethylacetoacetate (CAS 141-97-9 Fluka) in 1:1 volume ratio during 20 min. Then the solution was hydrolysed during 1 h in presence of 0.32 M nitric acid aqueous solution. GPTMS was mixed with 2-propanol in 1:1 volume ratio. The solution was hydrolysed in the nitric acid solution with a 0.13 volume ratio of water to GPTMS under stirring during 1 h. Both TPOT and GPTMS containing solutions were mixed together for one additional hour and then left ageing for another hour. The synthesis process was carried out at a temperature 22 ± 1 °C maintained by a water circulating thermostat.

LDH layer synthesis and sol-gel coating processes are schematically presented in Figure 1. Sol-gel coatings were applied on the LDH treated AA2024 plates using a dip coating process. The plates were immersed for 100 sec in a sol-gel solution and then withdrawn at a speed of 18 cm/min. After drying in air during 30 min the coated samples were transferred to a pre-heated oven at 120 °C where they were cured during 80 min.

Vanadate analytical release studies were performed using standalone sol-gel film which was prepared by mixing hybrid sol-gel formulation (synthesized as described above) with LDH(V2O7) powder (synthesised by co-precipitation method [4]) which was cast onto Teflon moulds and cured using the sol-gel curing process described above. The final dry weight loading of LDH in the cast films was about 18 wt.% which was determined by the difference between the weight of a pure sol-gel and the sol-gel mixed with LDH powder.

2.3 SEM/EDS

Scanning electron microscopy/energy dispersive spectroscopy (SEM/EDS) studies were performed with Hitachi S4100 FE-SEM and Hitachi Su-70. All samples were sputtered with a carbon layer to provide surface conductivity.

2.4 EIS

Electrochemical impedance spectroscopy (EIS) measurements were performed with a Gamry FAS2 Femtostat with PCI4 controller at open circuit potential with 10 mV RMS applied sinusoidal perturbation in a frequency range of 2.6×10^{-3}-1×10^{5} Hz with 7 data points per frequency decade. The electrochemical cell consisted of a saturated calomel reference electrode (SCE), a counter platinum spring electrode, and a coated AA2024 sample with a surface area of 3.35 cm^2 working electrode. The measurements were carried out in 0.5 M NaCl (CAS 7647-14-5 Sigma-Aldrich) solution at open air at a temperature about 22±1 ºC in a Faraday cage. Impedance spectra were treated using EchemAnalyst (Gamry Inc.) software.

2.5 SVET

An Applicable Electronics (USA) Scanning vibrating electrode technique (SVET) was used for measurements of ionic current densities. The SVET microprobe presents a spherical platinum black tip with 10 µm of diameter. The tip is being vibrated in a direction normal to the surface at a vibration frequency around 89 Hz and with amplitude around 20 µm. The technique is based on measurement of potential gradients in solution associated to ionic fluxes created by oxidation and reduction reactions on the metallic substrate. The measured voltage differences were converted to current densities (normalized for 1 cm^2) by a calibration routine.

The samples were glued on plastic holders and sides of AA2024 were insulated with bee's wax, with leaving only the sol-gel covered measurable area of approximately 4x4 mm exposed to the corrosive media of 0.05M NaCl solution. Ionic current measurements on sol-gel coated samples were obtained with the probe vibrating at a distance of 100 µm above the sample surface during the immersion. Maps of ionic currents with 40x40 data points were measured systematically at different time intervals. SVET data treatment and analyse was done with contribution of data analysis package by LocalProber (Estonia) SVET equipment.

2.6 GDOES

Glow discharge optical emission spectroscopy (GDOES) depth profile analysis of coatings was conducted with a HORIBA GD-Profiler 2. Radio frequency plasma discharge with 40 W input power was ignited between the sample and 4 mm copper anode at 650 Pa argon operating pressure. The plasma discharge sputtered the sample surface and optical emission spectra of the elements present in the coating were evaluated during the etching process. Each sample was measured at least in 3 different places in order to have reproducible results.

2.7 UV-Vis Spectroscopy

Detection of Vanadate species was performed using UV-Vis Spectrometer at 260-267 nm wavelength using modified methodology from the literature [30]. The modification consists of the Vanadate species detection at pH 10 in a buffered solution (Buffer solution, pH 10, transparent, Alfa Aesar Specpure). The concentration of Vanadate species in the solution with unknown concentration has been calculated using the calibration curve obtained from a set of standard concentrations of vanadate solutions measured under the same conditions ($R^2 = 0.9839$). All the measurements were done in triplicate.

The liquid samples were prepared by mixing 10 ml of 0.5M NaCl solution with about 0.043 g of pure LDH(V2O7) powder or 0.240 g of cast sol-gel/LDH(V2O7) film in plastic containers. The liquid mixture was stirred at 200 r.p.m. at room temperature. At a certain time 1 ml aliquot was taken from the mixtures and diluted with 1 ml of buffer pH 10. The aliquot was preliminary filtrated using 3 ml syringe and filter with 0.45µm pore volume in order to remove any solid contaminants. The taken aliquot was replaced with a clear 1 ml of 0.5M NaCl solution in the initial mixture to maintain the total volume of liquid part in the mixture. After 1 h of aging the aliquot (this time is sufficient for vanadate speciation form equilibrium achievement, corresponding to pH 10, namely, VO_3), the measurement of vanadate absorption was performed in a 10 mm quartz cuvette, using pH 10 buffer solution as a blank solution.

3. Results and discussion

3.1 Microstructural and chemical analysis

Figures 2 (a,b) depict surface microstructure of AA2024 after two cleaning pre-treatments, namely #1 (two-step process) and #2 (three-step process). In the course of the pre-

treatments a fraction of intermetallics is being dissolved. While a small part of intermetallics was removed from the surface after pre-treatment #1 (Figure 2a) the second pre-treatment #2 (Figure 2b) significantly reduces the population of intermetallics on the metal surface. This is clearly displayed by a lot more craters formed on the surface after dissolution of intermetallics. By reducing the content of intermetallics on the alloy surface the corrosion resistance of the aluminium matrix increases. On the downside the presence of intermetallics is directly related with the growth of LDH on AA2024 surface.

Figures 2 (c,d,e,f,g) present surface microstructure of the sol-gel coated samples with or without LDH. The micrographs show LDH islands (brighter places) over coated by sol-gel and surrounded by sol-gel matrix (darker zones). Several distinct features can be seen. The 2-step process (#1) produces a more abundant LDH islands on the metallic surface (Figure 2 c,e) compared with the 3-step process (#2) (Figure 2 d,f). In addition, in the case of a 2-step process cracks appear atop the LDH islands as can be seen in the inset of Figure 2c. Such cracks could not be observed on other samples. It can be speculated that the residual solvents (water and/or 2-propanol) may penetrate deep into the LDH islands and during the sol-gel coating curing process and cause large amount of stress in the sol-gel matrix atop the LDH islands thus causing cracks in the coating. EDS analysis made at the LDH islands clearly demonstrates Zn signal which is attributed to the LDH (Figure 2h). Al signal comes from LDH and the substrate. Vanadium signal clearly corresponds to incorporated species of vanadates in LDH. It has been shown before that the LDH with incorporated vanadate species grown on AA2024 surface contain Al, Zn, V and O elements [19]. The peaks assigned to Zr, Si and O represent composition of the sol-gel matrix after curing. In contrast to LDH containing samples, the reference sol-gel coating microstructure does not show any cracks (Figure 2g). The sol-gel coating homogeneously covers the alloy surface.

The effect of surface pre-treatment on the growth of LDHs has been discussed in a previously work reported by our group [31]. In particular, the effect of these pre-treatments was discussed in the detail in terms of surface morphology and electrochemical properties. The industrial-based pre-treatment (#2) removes the machined (mechanically deformed) layer from the AA2024 surface and the intermetallic particles, making the aluminium oxide layer more stable and thick when compared to the lab-based pre-treatment (#1), which is less effective in this regard. This difference, explains a higher coverage of LDHs in the (#1) pre-treatment because the substrate will provide higher amounts of aluminium species when compared to the (#2) pre-

treatment, thereby co-precipitating with Zn^{2+} from the solution into a LDH structure. With a higher LDH surface coverage, more corrosion inhibitor is available to provide corrosion inhibitor in demand.

Figure 3 presents cross-sections of #2LDH(NO3) and #2LDH(V2O7) samples embedded in resin. The images were acquired at places where LDH "bushes" can be clearly seen on AA2024 surface (Figure 3a,f). The structure of LDH layer (composed of Zn, Al and partially O) is clearly seen at the central part of the coating. A V signal is preferentially found at LDH places suggesting a stable interconnection with the LDH structure. LDH coatings obtained in this work have similar properties as in the previous study where a more detailed characterisation of cross-sections of LDH coatings on AA2024 surface was given [19]. The LDH structure includes pyrovanadate ions which are composed of linked tetrahedra (VO_3–O–VO_3) [32]. When such anions are arranged parallel to the brucite layers plane the gallery height was about 0.5 nm. The gallery height for LDH with intercalated ($V_2O_7^{4-}$) estimated from the XRD data was about 0.47 nm [19, 32]. Elemental maps of Si, Al, Zn, O and V reveal the composition of the sol-gel and LDH layers. It can be easily deduced that the sol-gel matrix effectively penetrates the porous LDH structure since Si, Zr and (partially O) elements can be clearly seen at LDH zones. It appears that the coating thickness slightly increases at big LDH islands compared with the outside zones.

3.2 Electrochemical impedance spectroscopy

Corrosion behaviour of the sol-gel coated samples was evaluated by EIS during immersion in 0.5 M NaCl solution. Impedance spectra of samples after 1 and 14 days of immersion are presented in Figure 4. The samples having LDH layers prepared on the 2-step and 3-step cleaned AA2024 surface show slightly different EIS spectra at the beginning of immersion. Typically, the EIS spectrum of a sol-gel coated AA2024 substrate has a time constant associated with the sol-gel coating dielectric properties and pore resistance, another time constant is associated with the dielectric properties and pore resistance of the intermediate oxide layer and the last one is associated to the charge transfer resistance and double layer capacitance [33, 34]. The first two time constants are clearly seen on the spectrum of Control sample (Figure 4a) at about 10^3 – 10^4 Hz and about 10^{-1} Hz respectively. For longer immersion times (ca. 14 days) a corrosion process time constant clearly shows up on the Control sample spectrum at about 10^{-2} Hz (Figure 4b).

When analysing the spectra after the first day of immersion, one can clearly see that the samples with LDH layers have one additional time constant developed at the middle frequency range (near 10 Hz) (Figure 4a,c). This time constant can be associated with the mixed LDH and sol-gel layer. Such mixed layer can be observed on the substrates prepared according to #1 or #2 procedures (Figure 4c). At lower frequencies another time constant shows up, namely the one attributed to intermediate oxide layer (Figure 4a,c). At the very low frequency the corrosion process clearly manifests on EIS spectra after 1 day of immersion (Figure 4a). In general, impedance modulus |Z| is lower on samples prepared according to 2-step cleaned samples compared to 3-step cleaned one (Figure 4a,c). Mainly this effect is due to lower resistance (higher porosity and lower thickness) of the intermediate oxide layer. Among all the samples LDH(NO3) containing ones present the lowest impedance associated with the high corrosive activity. Sol-gel film resistance and mixed layer resistance drop and corrosion process clearly appears at low frequency after 14 days of immersion (Figure 4b,d). However, LDH(V2O7) containing samples demonstrate that the phase angle at low frequency corresponding to the corrosion process time constant is lower than for Control and LDH(NO3) systems. The EIS spectra of the latter two samples show resistive response at low frequency.

A further analysis of EIS spectra was made using EIS numerical fitting process in order to extract physical parameters describing the studied electrochemical systems. Equivalent circuit models presented in Figure 5 were employed for fitting. The models include the following elements: sol-gel coating's porosity R_{coat} and capacitance Q_{coat}, R_{mixed} and Q_{mixed} elements describe LDH/Sol-gel layer, R_{ox} and capacitance Q_{ox} elements describe barrier oxide layer properties, and R_{ct} and Q_{dl} describe charge transfer resistance and double layer capacitance of corrosion process. The electrolyte resistance is not clearly seen on EIS spectra, though this element was included in the equivalent circuits in order to provide a better goodness of fitting. The models include constant phase elements (CPE) instead of capacitors. This has been done due to non-ideal impedance response of the coatings and electrochemical processes which show dispersions of time constants [35]. Such dispersive behaviour can be attributed to inhomogeneous surface and thickness, and distribution of coating's dielectric properties.

The equivalent circuit model (Figure 5a) has been used for fitting EIS spectra of aluminium alloys coated by sol-gel films [23, 33, 36, 37]. The model (b) is somewhat more complicated and includes an additional time constant element describing properties of the mixed layer (Figure 5b). Such mixed layer consists of LDH mixed hydroxides intercalated with the sol-

gel matrix (Figure 3). A clear distinction between such a layer and a sol-gel coating can be made if one compares EIS spectra fitting taken at the beginning of immersion. The selected equivalent circuit models were similar to those presented in Figure 5 with one exception. Fitting results of the studied coating systems, namely Control, #1LDH(NO3), #1LDH(V2O7), #2LDH(NO3) and #2LDH(V2O7) after 1 hour of immersion are presented in Table 2. Initial coating resistance is lower for (NO3) containing systems. A Q_{coat} parameter of the Control sample is about 3.4×10^{-8} ($S\cdot s^{a}\cdot cm^{-2}$) this parameter is slightly lower for #1LDH(V2O7) or (#1LDH(V2O7)) about 2.41×10^{-8} and (2.25×10^{-8}) and higher for #1LDH(NO3)/#2LDH(NO3) about 2.59×10^{-7} and (7.93×10^{-8}) respectively. Both LDH(NO3) samples have higher Q_{coat} than other systems and such discrepancy can be caused by different rate of water absorption and hydrolytic instability of the coatings during immersion. The mixed layer CPE element parameter Q_{mixed} is relatively high about 1×10^{-6} - 3×10^{-6} ($S\cdot s^{a}\cdot cm^{-2}$) (Table 2). Since the mixed layer consists of inorganic (mostly hydroxides) and sol-gel parts it is expected to have a higher capacitance. Oxide layer resistance R_{ox} is lower in case of nitrate containing samples vs. Control and vanadate containing ones (Table 2). Also, the fitting displays the presence of corrosion process on #1LDH(NO3) and #2LDH(NO3) samples. Overall the behaviour of LDH(NO3) samples emphasises poor protective capabilities vs. other systems. A further EIS spectra analysis will present how the most significant fitting parameters change in the course of immersion.

Figure 6 presents kinetics of evolution of different fitting parameters during immersion. Sol-gel coating resistance (R_{coat}) decreases during immersion time with approximately similar rate for different coating systems (Figure 6a). The decrease is mostly associated with appearance of micro pores in the coatings during immersion. Next, the evolution of mixed layer resistance (R_{mixed}) is presented in Figure 6b. Two clear tendencies can be seen the coatings having LDH(NO3) layer demonstrate almost an order of magnitude lower resistance compared with the systems having LDH(V2O7) layer. It can be seen that the type of cleaning process (whether it is #1 or #2 Table 1) does not affect the resistance of the mixed layer. This fact may suggest that the LDH(V2O7) coating is much denser and more resilient towards the water penetration. On the other hand the coatings containing LDH(NO3) show excessive cracks and imperfections on the surface (Figure 2a). These features clearly have a negative effect on the mixed layer resistance.

Intermediate oxide layer is in the vicinity of the metal surface and can be directly subjected to corrosion process. Arguably, the high resistance and low capacitance of such layer testify for a higher protectiveness of the coating system. In this work two pre-treatments were

investigated which give raise to different microstructure of the alloy surface (Figure 2) and also different passive oxide film properties. The industrial-based pre-treatment (#2) removes much more intermetallics on the surface making a thicker aluminium oxide layer when compared to the lab-based pre-treatment (#1).

Figure 6c presents evolution of oxide layer resistance (R_{ox}). At the very beginning of immersion the values of R_{ox} were similar for Control, #1LDH(V2O7) and #2LDH(V2O7) systems (about 6-10 $M\Omega cm^2$) and 1 or 2 orders of magnitude higher than #1LDH(NO3) and #2LDH(NO3) systems. Although the surface having pre-treatment #2 contains fewer intermetallics the #2LDH(NO3) sample does not enforce oxide layer resistance. This procedure produces a defected oxide layer. On the other hand, #1LDH(V2O7) sample, having intrinsically more intermetallics on the surface, displays a relatively high oxide resistance (Figure 6c). This is associated with the strong passivating role of vanadate inhibitor which may patch up defects in the oxide layer to such extent that the R_{ox} keeps high. After a few days of immersion the resistance has significantly decreased especially for LDH containing systems. During initial immersion a corrosion process may have started and caused some disruption of the oxide film and consequently R_{ox} has decreased. However, at longer immersion time the resistance had consistent stable values. The ranking of the oxide layer resistance at long immersion time is as follows: Control ≈ #2LDH(V2O7)> #1LDH(V2O7)> #2LDH(NO3)> #1LDH(NO3). Clearly, the LDH(V2O7) systems have a higher oxide resistance compared with the LDH(NO3) ones due to active role of the inhibiting anions towards the destruction of the oxide layer. This dependence also reveals that the alloy cleaning process #2 provides a higher oxide layer resistance of the sandwich system compared with the #1 cleaning process. However, other parameters such as R_{coat} and R_{mixed} did not show any dependence on whether #1 or #2 cleaning process was used.

The oxide capacitance can also enlighten the behavior of the oxide layer during immersion. Since the CPE parameter (Y) does not have the dimensions of real capacitance a procedure is needed to convert a Q parameter to real capacitance. This problem has been widely discussed in different papers [38-40]. For example, Hsu and Mansfeld proposed to use equation (1) in the case of parallel connection of CPE and R. For a normal distribution of time constants which results in a distributed time-constant behavior the effective capacitance associated with the CPE can be expressed by the equation (2) (Brug formula (5) [39]). However, in case of a surface time-constant distribution (Brug formula (20) or Hirschorn formula (11) apply [39, 40]) which can be expressed by the equation (3).

$$C_{eff} = Q(\omega_{max})^{(\alpha-1)}, \quad (1)$$

$$C_{eff} = Q^{1/\alpha}\left(R_f\right)^{(1-\alpha)/\alpha}, \quad (2)$$

$$C_{eff} = Q^{1/\alpha}\left(\frac{ReRf}{Rf+Rf}\right)^{(1-\alpha)/\alpha} \quad (3)$$

where, C_{eff} is an oxide capacitance expressed in ($F \cdot cm^{-2}$), Q and α are CPE parameters, ω_{max} is a frequency at which the imaginary impedance attributed to a certain time constant has maximal value, R_f is the resistance of a film, R_e is Ohmic resistance. Oxide layer capacitance (C_{ox}) was calculated using the equation (3). It was assumed that the oxide time-constant shown on EIS spectra is the result of time constants distributed along the metal surface. Figure 6d presents evolution of C_{ox} versus immersion time. In general, all four LDH systems show approximately the same initial capacitance (about 0.7×10^{-6} $F \cdot cm^{-2}$) vs. about 2×10^{-6} $F \cdot cm^{-2}$ for the Control system. The capacitance does not significantly change during immersion except for #1LDH(NO3) sample which shows a rapid increase and then monotonous decrease (Figure 6d). The capacitance depends on the total area of the oxide film in contact with the electrolyte solution and on the thickness of the film. The higher the oxide layer area and the thinner the oxide the higher is the oxide layer capacitance. For electrochemical systems a thinner oxide layer or a larger surface exposed to corrosion is detrimental from the point of corrosion protection of the metal surface. The three systems #2LDH(V2O7), #1LDH(V2O7) and #2LDH(NO3) showed lower capacitance and therefore the highest protectiveness.

Charge transfer resistance (R_{ct}) evolution during immersion is presented in Figure 6e. This parameter represents active electrochemical process occurring at the metal surface. At the beginning of immersion LDH containing systems showed R_{ct} within $1\text{-}5\times10^5$ Ωcm^2 while the corrosion process was not detected on Control sample. However, by the end of 160 hours of immersion R_{ct} of #1LDH(V2O7) and #2LDH(V2O7) increased until about 1×10^8 Ωcm^2. At longer immersion time #2LDH(V2O7) system showed R_{ct} drop till about 1×10^7 Ωcm^2. However, #1LDH(V2O7) system demonstrated some decrease followed by a consistent increase of R_{ct} till about 2×10^8 Ωcm^2. On the other hand, the nitrate containing systems #1LDH(NO3) and #2LDH(NO3) showed more than an order of magnitude lower R_{ct} ($2\text{-}7\times10^6$ Ωcm^2) than LDH(V2O7) systems. The growth of R_{ct} may suggest a healing of the corrosion process at the alloy surface.

Both inhibited systems showed a much higher resistance than the Control system and uninhibited ones. At this point it can be concluded that the inhibited systems demonstrated an

efficient long term corrosion protection of AA2024. It should be pointed out that when the cleaning process #1 is used the R_{ct} tends to be higher at longer immersion time in contrast to the cleaning process #2 in which R_{ct} decreases. This discrepancy can be correlated with the microstructural properties of the samples prepared with #1 and #2 processes. The samples pretreated following the first pre-treatment process have larger distribution of LDH over the metal surface compared with the second one. Therefore, the larger the LDH distribution at the surface the more vanadate inhibitor will be incorporated during the anionic exchange. This may explain the observed discrepancy in R_{ct} at longer immersion. The next step was to understand what would be corrosion activity of the LDH containing systems when the coating is disrupted and the metal surface is directly exposed to a corrosive electrolyte.

3.3 SVET studies

Measurements of local ionic current densities have been done using SVET on the coated samples containing of two circular sharp needle made defects that penetrated the coatings to the metal surface. Ionic current maps acquired at different immersion times in NaCl solution on Control, #2LDH(NO3) and #2LDH(V2O7) samples (as an example) are depicted in Figure 7. After short term of immersion a weak anodic and cathodic activity shows up on Control sample. During further immersion the ionic currents grow achieving the values about +62 and -7 μAcm^{-2} for anodic and cathodic corrosion respectively after 1 week of immersion (Figure 7). A smaller cathodic activity may be related with the fact that a part of the cathodic activity takes place at the anodic pitting site and at the metal surface in pores of the sol-gel coating on the large area of the sample. The generated hydroxyl anions due to cathodic process may not come into the plane of vibration of a SVET probe which provides limitations for detection by the probe. However, as the anodic and cathodic electrochemical processes are linked, the changes of the anodic activity were used for interpretation of active healing action. The anodic activity correlates with the place of a pit covered with corrosion products clearly visible on the optical picture. Samples #2LDH(NO3) and #2LDH(V2O7) demonstrate quite different behaviour. At the beginning of immersion a high anodic activity develops at one of the defects on both samples. Remarkably, this activity is about ten folds higher on #2LDH(NO3) sample (132 μAcm^{-2}) compared to #2LDH(V2O7) one (13 μAcm^{-2}). Although the magnitude of ionic current decreases on #2LDH(NO3), the optical images of the sample confirm high corrosion activity and abundant corrosion products development at the place of the anodic activity (Figure 7 optical image), contrary to that, the anodic activity

measured on #2LDH(V2O7) sample slightly decreases over time. During the initial days of immersion the LDH coating does not provide defined inhibition due to possible lack of inhibitor at defect locations. However, at the end of immersion period (1 week) neither anodic nor cathodic activities were detected on ionic current maps. The decrease of current densities at defects may be explained by self-healing effect of LDH(V2O7) in corrosion protection of AA2024. The optical image of the surface of #2LDH(V2O7) sample after immersion also confirms absence of any corrosion product precipitates signifying well-defined corrosion inhibition. The presented experimental series for #2LDH(V2O7) is selected the worse one, where initially the currents occurred and only later disappeared during the immersion time, in order to show the possible self-healing effect. While in case of other experiments the #2LDH(V2O7) often shows a good corrosion protection and no detectable activity since the beginning of immersion.

3.4 Surface analysis after immersion tests

Figure 8 presents SEM images of #2LDH(NO3) and #2LDH(V2O7) containing coatings after EIS measurements taking almost a month of immersion in 0.5 M NaCl solution. The pictures show significant cracking at the places of mixed hydroxides (bright islands) in both LDH(NO3) samples (Figure 8a,c). On the contrary, the LDH(V2O7) samples demonstrate only a few micro cracks located at the mixed hydroxide places (Figure 8b,d). The existence of cracks is very much consistent with EIS measurements demonstrating a loss of sol-gel barrier protection and a significant decrease of mixed layer resistance during immersion of LDH(NO3) samples (Figure 6a,b). On the other hand, these two parameters were higher for LDH(V2O7) containing coatings. The chemical analysis performed at the islands of mixed hydroxide layers suggested changes in chemical composition. Figure 8e shows EDS spectra acquired at LDH islands of LDH(NO3) and LDH(V2O7) samples. The spectra show typical elemental composition of the sol-gel coatings (Si, O, Zr), double hydroxides of (Al and Zn) and a (V) signal highlighting the incorporated inhibitive species. In addition the Cl signal, with higher intensity on LDH(NO3) sample, appears on both samples. Such signal can be detected on all LDH containing systems after corrosion testing. Therefore, the accumulation of Cl in the LDH islands can be correlated with anion exchange occurring between the LDH and chloride anions and/or desorption of vanadate inhibitor from LDH.

An additional chemical analysis of the coatings has been performed by GDOES. Figure 9 presents GDOES elemental profiles obtained on #2LDH-NO3 and #2 LDH(V2O7) samples

before and after 1 month of immersion in 0.5 M NaCl. These elemental profiles were obtained simultaneously during the coating sputtering in the plasma discharge. During the sputtering the surface is gradually removed while chemical composition of the plasma is analysed. There are three main regions that can be highlighted on the profiles. Before immersion the first region (zone I) shows distinct footprints of the sol-gel coatings consisting of Si, Zr and O elements (Figure 9). The intensities of these signals decrease with sputtering time. On the other hand the signals representing the LDH layers (zone II), namely Zn (V in case of LDH(V2O7)) increase when going closer to the metal/coating interface and then decrease. Such behaviour is most probably attributed to the fact that LDH is directly grown at the metal surface and is partially coated by a sol-gel coating. Thus at initial sputtering times the signal increases when plasma reaches the LDH bulk, and then decreases when most of the LDH has been etched away. Al signal, on the contrary, increases mostly due to contribution from the LDH layer and from the alloy composition. The transitionary region is near the metal surface. At this place both signals from the coating and the alloy can be seen on the profiles (Figure 9). When plasma reaches the alloy surface (zone III) a Cu signal clearly shows up on the profiles (Figure 9). The last zone corresponds to the bulk alloy, which mostly shows copper and aluminum signals, characteristic elements of AA2024 composition. After immersion the shape of profiles of most of the elements remained the same. However, a new element can be identified, namely Cl, which is included in the coating layer in the course of immersion in NaCl solution. The intensity of Cl signal is higher for LDH(NO3) sample than LDH(V2O7). This result is very well consistent with the EDS analysis presented above indicating a higher Cl signal on the sample containing LDH nitrate.

3.5 Analytical studies of vanadate inhibitor release

Release studies could not be done on AA2024 coated by LDH(V2O7) sol-gel due to interference of the alloy with the release of vanadate species which can efficiently adsorb on the metal. Therefore, model experiments were conducted with Zn/Al LDH(V2O7) particles synthesized by conventional anion-exchange procedure using Zn/Al-nitrate LDH as the precursor [5] and incorporated into the same sol-gel formulation. The sol-gel was cast into Teflon moulds and cured. The final dry weight loading of LDH in the coating was about 18 wt.% which was determined by the difference between the weight of a pure sol-gel and the sol-gel with LDH powder. Both LDH(V2O7) grown on metallic AA2024 and LDH(V2O7) powder synthesised via

co-precipitation route have high extent of similarity in terms of structural and morphological features. The last fact was confirmed in paper [19]. Tedim et al. showed similarity of XRD characteristic reflections positions of LDH(NO3) and LDH(V2O7) grown on metallic substrates with the same structural polycrystalline LDHs prepared by co-precipitation route [32]. The plate-like crystal morphology of deposited LDHs is also in agreement with previous published work [5].

Figure 10 presents vanadate release profiles of the two systems, namely LDH powder and sol-gel coating with LDH. In studied conditions (buffer pH 10) the predominating speciation of V is VO_3 [41]. As a corrosion trigger the solution of 0.5M NaCl was used. The studies of Tedim et al., 2012 (J. Tedim, A. Kuznetsova, A.N. Salak, F. Montemor, D. Snihireva, M. Pilz, M. L. Zheludkevich, M.G.S. Ferreira/ Zn–Al layered double hydroxides as chloride nanotraps in active protective coatings// Corrosion Science 55, 2012, pp. 1–4.) showed, that concentration of released anions from LDH increases with the increment of sodium chloride concentration in bulk solution. Thus, for tests high concentration of sodium chloride was chosen: to provide the high extent of exchange with vanadate anions.

The release of inhibitor from LDH-powder is fast, achieving a maximum during first 24 h with slight decrease of released values for long timescale (more than 1 week). It was calculated that during release timescale (4 weeks in presence of 0.5M NaCl) the released vanadate value from the LDH powder corresponds to around 4% from the loading content. The loading content of vanadate in LDH is about 10% wt. This concentration decrease can be associated with possible adsorption of vanadate on the LDH-surface. According to the literature data BET surface area of different types of synthesized LDH varies in the range of 1-3 m^2/g depending on the types of cations in LDH structure [42]. Studies of Abdolmohammad-Zadeh et al. showed the successful application of Zn/Al-LDH as good sorbent of organic dye [43]. Another justification for this can be the precipitation of vanadate in some sort of insoluble salt ($Zn_3(VO_4)_2$) which is retained in the filter or in the powder.

Sol-gel coating with incorporated LDH shows a slow kinetics of vanadate release, which is about 15 times lower in comparison to LDH powder (Figure 10). The accessibility of chlorides defines the exchange rate with vanadate anions in the LDH structure. Transport properties and permeability of organic coating towards moisture and, in particular, chloride species create additional limitation for the vanadate release [44, 45]. The main conclusion is that sol-gel reduces kinetics of release of vanadate species. This helps to keep the inhibitor in LDH and prolong

corrosion inhibition. In order to provide a better release a defect in the coating should be made which would provide an impetus for anionic exchange with chloride anions. The latter mechanism has been proven by SVET analysis.

Additionally, the replicas solutions containing sol-gel coating with LDH system after the last point measurements were analysed by ICP-OES analysis. The average concentration of vanadate (VO_3 form) was about 2.2±0.3 ppm, which is at the similar level as was estimated by UV-Vis spectrometry (Figure 10).

3.6 Mechanism of inhibition

Sol-gel coatings had been explored as possible pre-treatment for aluminium alloys before. Given the high flexibility of sol-gel chemistry to impart different properties to the sol-gel coatings the latter may also be employed as a primer coating to improve adhesion. Besides, a sol-gel matrix, provided that it is thick enough, may be used for storage of inhibitor containers thus granting the coating a role of a primer in the multilayer protective systems. In this work a simple sol-gel formulation in conjunction with the LDH layers has been used to demonstrate its efficiency in corrosion protection of AA2024. The coating is able to provide the reinforcement of the interface between the metal and LDH by forming a transitory region with the sol-gel coating. This coating would fill defects and improve adhesion between the metal and LDH, besides providing chemical interlink with organic layers. When defects appear in the coating the corrosive electrolyte would permeate down to metal causing uncontrollable corrosion. However, the sub LDH layer would release the inhibiting species into the defects thereby curbing the starting corrosion process.

Electrochemical tests, namely EIS and SVET, clearly demonstrate an efficient corrosion inhibition of AA2024 coated by LDH(V2O7) systems (Figures 6,7). Particularly, charge transfer resistance calculated for LDH(V2O7) systems (about 10^8 Ωcm^2) was at least one order of magnitude higher than that for other systems (about 10^6-10^7 Ωcm^2). Ionic current densities measured by SVET at two defects were effectively suppressed in the inhibited system (anodic currents from 13 µ μAcm^{-2} to about 1-2 μAcm^{-2}) compared with the control sol-gel coated alloy (anodic currents from 3 μAcm^{-2} to about 62 μAcm^{-2}). Inhibition of cathodic corrosion at AA2024 can be clearly seen in SVET results which detect only anodic ionic currents in artificial defects made on #2LDH(V2O7) layers (Figure 7). However, following the dynamics of ionic current

changes measured at the defects of LDH(V2O7) layers it can be seen after 7 days immersion the currents dropped to almost zero (Figure 7) thereby demonstrating a very efficient self-healing process. Such corrosion protection is clearly provided by high effectiveness of vanadate species for corrosion inhibition of AA2024.

The corrosion inhibiting efficiency of LDH(V2O7) depends not only on the release rate on the vanadium species but also on the chemistry of the corrosive environment. Vanadate species, unlike many others, have different speciation in solutions with different pH [41]. In acidic solutions vanadate species tend to polymerize forming polyanions octahedral vanadates. In a defect, which shows mostly anodic dissolution of aluminium, pH decreases due to hydrolysis of Al^{3+} cations and at high dissolution rates the pH values may be about 3 or lower [46]. At such conditions it is expected that vanadate species polymerise forming much less effective decavanadate species [47]. On the contrary, at higher pH simple tetrahedral vanadate species are formed [41, 47-49]. These species provide more effective inhibition than octahedral species. An extensive study on the correlation between different structure of vanadate species and their inhibiting performance has been done [41, 47, 48]. Vanadate species provide cathodic corrosion inhibition of oxygen reduction reaction following the adsorption at active intermetallics and reduction at cathodic metal surface [47]. It has been established that local breakdown and dissolution of active intermetallics such as S-phase (Al_2MgCu) is prevented in vanadate solutions at high pH [41, 50]. Also it was reported that pitting potential of pure aluminium increased, though anodic passive currents were higher on aluminium in NaCl + $NaVO_3$ solution than in NaCl one [50]. In terms of inhibiting efficiency performance tetrahedral vanadate species have higher performance compared to octahedral ones. Vanadate species and their inhibiting performance can be arranged in the following way: V1>V2>V4>V10. Therefore, a preferable scenario of inhibition may include release of tetrahedral vanadate species providing more efficient corrosion inhibition in cathodic defects.

Release studies indicated that the concentration level of vanadate species released from the sol-gel coating containing LDH is quite small (about 1 ppm (0.01 mM)). At such concentration it is expected to have the following species at equilibrium $VO_2(OH)_2^-$, $VO(OH)_2^-$ in the range of pH from 5 to 9 [41] and a reference in that paper [51]. Iannuzzi et al. reported that monovanadate species provide efficient corrosion inhibition of AA2024 already at a concentration about 0.007 mM in aerated solution at pH 7.6 [47]. At concentrations higher than 0.02 mM the calculated inhibiting efficiency was higher than 90% [47]. In spite of a low

concentration of vanadate species detected by analytical studies in this work, the concentration near the surface and especially in microdefects in the coating should be higher as the LDH coating is located directly in contact with the metallic surface. The concentration of vanadate released from LDH powder is about 20-30 ppm (0.2 – 0.3 mM) (Figure 10). Although sol-gel coating containing LDH releases less inhibitor than the LDH powder, when the coating is damaged the LDH conversion layer will have capabilities to release sufficient quantity of inhibitor in the defect. It is also reasonable to assume that the inhibitor released form the conversion layer needs less traveling time to the metal surface in order to provide effective corrosion inhibition.

LDH containers may also contribute to corrosion inhibition of AA2024 by the anionic exchange process with aggressive anions such as Cl^-. When chlorides uncontrollably diffuse and concentrate at the aluminium surface they adsorb on the passive oxide surface and penetrate through the oxide film via vacancy transport and cause localized dissolution of aluminium at the metal/oxide interface [52]. The formation of transitory compounds within the oxide film contributes to the inhibition of the anodic dissolution of the native film-covered pure aluminium below the pitting potential [53]. However, at potentials higher than pitting potential these compounds dissolve into solution thus causing pitting. The reduction in adsorption of Cl^- by other anions (e.g. NO_3^-, SO_4^{2-}) was found to increase pitting potential and reduce overall corrosion on Al surface [53, 54]. LDH may effectively exchange NO_3^- for Cl^- anions during immersion in NaCl solutions [55]. Having that in mind, both LDH(NO3) and LDH(V2O7) can contribute to corrosion protection of AA2024 by adsorbing corrosive chloride anions. This effect may be responsible for increasing the charge transfer resistance of LDH(NO3) samples as has been evaluated by EIS (Figure 6e). Though the impact of Cl^- trapping is much smaller for LDH(V2O7) system which did not show high chloride content after immersion (Figure 9). The latter is associated with slow kinetics of anion exchange between the incorporated vanadate and chloride anions. At such slow anionic exchange the leaching rate of the inhibitor is quite low which is beneficial for keeping the inhibitor in the coating. However, the coatings systems including LDH(NO3) layers adversely affected sol-gel barrier properties causing extensive corrosion of the alloy. They also failed to show active corrosion protection in SVET tests.

After gathering all the information a scheme presenting a possible mechanism of vanadate release from LDH structures and corrosion inhibition at AA2024 can be shown (Figure 11). The surface of AA2024 contains cathodic intermetallics which support oxygen reduction process [47].

Since the cathodic process is balanced by an anodic process of aluminium oxidation the extensive corrosion inevitably leads to development of pitting corrosion. During immersion in NaCl solution vanadate anionic species in LDH structure release, diffuse into the solution near defects and adsorb preferably on the cathodic intermetallics thereby inhibiting cathodic process of oxygen reduction. The cathodic inhibition leads to decrease in anodic activity and thus improving the corrosion resistance of AA2024 in NaCl solution. Localized corrosion inhibition can be traced down to independent intermetallics which extensive dissolution is prevented in the course of immersion in the NaCl solution (Figure 11). These results are in line with other works presenting localized inhibition of intermetallics corrosion [50, 56, 57]. Similarly, LDH(NO3) layers may effectively scavenge Cl^- anions which may reduce corrosion process at AA2024 surface. However, in this work EIS and SVET electrochemical measurements did not show efficient corrosion protection of AA2024 by LDH(NO3) conversion layers. One of the main limitations of these layers is their high tendency to form defects in the sol-gel coatings as was revealed by EIS fitting results (Figure 6a,b) and microstructural analysis (Figure 8a,c). On the other hand, LDH(V2O7) coatings do not destroy sol-gel matrix and provide efficient active corrosion protection with defined self-healing.

5. Conclusions

In this work corrosion protective properties of two layer sandwich systems consisting of a LDH conversion layer covered by a sol-gel coating were explored.

Coating systems containing LDH(NO3) conversion layers caused significant damage in the sol-gel coating after immersion which was observed in microstructural studies. Impedance results showed weak barrier protection of sol-gel coatings and mixed layers and high localized corrosion activity displayed by SVET measurements.

On the other hand, coating systems containing LDH(V2O7) conversion layers demonstrated clear microstructure without visible microdefects before and after immersion in 0.5 M NaCl solution. LDH(V2O7) conversion layers are highly compatible with the sol-gel matrix and display higher mixed layer resistance unlike for LDH(NO3) ones. The coatings showed efficient active corrosion protection and self-healing abilities which were revealed by EIS and SVET studies.

Release studies showed very slow kinetics of vanadate release from the cast sol-gel/LDH(V2O7) coating matrix compared with the bare LDH(V2O7) powder. The slow release

can be associated with limited anionic exchange ability with corrosive chloride anions and diffusion limitations caused by the sol-gel matrix.

The corrosion protective mechanism of AA2024 by LDH coatings may involve two factors, namely scavenging of aggressive chlorides anions by LDH and release of corrosion inhibitive vanadate species to microdefects and effective cathodic corrosion inhibition at active metal surface provided by metavanadate species.

This study shows that it is possible to combine LDH and sol-gel coatings having active corrosion protection. This system has potential to be studied further as a part of a full protection system opening prospects for the development of new multilayer corrosion protection systems for aerospace applications.

Acknowledgments

KY thanks financial support of a Post-Doctoral grant (ref. SFRH/BPD/80754/2011) of the Portuguese Foundation for Science and Technology (FCT) and a researcher grant (IF/01284/2015). This work was developed within the scope of the project CICECO-Aveiro Institute of Materials, POCI-01-0145-FEDER-007679 (FCT Ref. UID /CTM /50011/2013), financed by national funds through the FCT/MEC and when appropriate co-financed by FEDER under the PT2020 Partnership Agreement. SK thanks FCT for researcher grant (IF/00856/2013) and ETAg for grant PUT1033. AK thanks the Portuguese Foundation for Science and Technology (FCT) in the form of a PhD grant (SFRH/BD/89490/2012). The present work was supported by MULTISURF European project (H2020-MSCA-RISE-2014-645676-MULTISURF).

References

[1] R.L. Twite, G.P. Bierwagen, Review of alternatives to chromate for corrosion protection of aluminum aerospace alloys, Progress in Organic Coatings, 33 (1998) 91-100.
[2] J. Sinko, Challenges of chromate inhibitor pigments replacement in organic coatings, Progress in Organic Coatings, 42 (2001) 267-282.
[3] R.G. Buchheit, H. Guan, S. Mahajanam, F. Wong, Active corrosion protection and corrosion sensing in chromate-free organic coatings, Progress in Organic Coatings, 47 (2003) 174-182.
[4] J. Tedim, S.K. Poznyak, A. Kuznetsova, D. Raps, T. Hack, M.L. Zheludkevich, M.G.S. Ferreira, Enhancement of Active Corrosion Protection via Combination of Inhibitor-Loaded Nanocontainers, ACS Applied Materials & Interfaces, 2 (2010) 1528-1535.
[5] M.L. Zheludkevich, S.K. Poznyak, L.M. Rodrigues, D. Raps, T. Hack, L.F. Dick, T. Nunes, M.G.S. Ferreira, Active protection coatings with layered double hydroxide nanocontainers of corrosion inhibitor, Corrosion Science, 52 (2010) 602-611.
[6] G. Williams, H.N. McMurray, Inhibition of filiform corrosion on organic-coated AA2024-T3 by smart-release cation and anion-exchange pigments, Electrochimica Acta, 69 (2012) 287-294.
[7] J. Mardel, S.J. Garcia, P.A. Corrigan, T. Markley, A.E. Hughes, T.H. Muster, D. Lau, T.G. Harvey, A.M. Glenn, P.A. White, S.G. Hardin, C. Luo, X. Zhou, G.E. Thompson, J.M.C. Mol, The characterisation and performance of Ce(dbp)3-inhibited epoxy coatings, Progress in Organic Coatings, 70 (2011) 91-101.
[8] M. Forsyth, T. Markley, D. Ho, G.B. Deacon, P. Junk, B. Hinton, A. Hughes, Inhibition of Corrosion on AA2024-T3 by New Environmentally Friendly Rare Earth Organophosphate Compounds, CORROSION, 64 (2008) 191-197.
[9] M. Kopeć, K. Szczepanowicz, G. Mordarski, K. Podgórna, R.P. Socha, P. Nowak, P. Warszyński, T. Hack, Self-healing epoxy coatings loaded with inhibitor-containing polyelectrolyte nanocapsules, Progress in Organic Coatings, 84 (2015) 97-106.
[10] H. Shi, L. Wu, J. Wang, F. Liu, E.-H. Han, Sub-micrometer mesoporous silica containers for active protective coatings on AA 2024-T3, Corrosion Science, 127 (2017) 230-239.
[11] J. Zhao, G. Frankel, R.L. McCreery, Corrosion Protection of Untreated AA-2024-T3 in Chloride Solution by a Chromate Conversion Coating Monitored with Raman Spectroscopy, Journal of The Electrochemical Society, 145 (1998) 2258-2264.
[12] X. Yu, C. Cao, Electrochemical study of the corrosion behavior of Ce sealing of anodized 2024 aluminum alloy, Thin Solid Films, 423 (2003) 252-256.
[13] H. Guan, R.G. Buchheit, Corrosion Protection of Aluminum Alloy 2024-T3 by Vanadate Conversion Coatings, CORROSION, 60 (2004) 284-296.
[14] A.S. Hamdy, I. Doench, H. Möhwald, Intelligent self-healing corrosion resistant vanadia coating for AA2024, Thin Solid Films, 520 (2011) 1668-1678.
[15] P. Campestrini, H. Terryn, A. Hovestad, J.H.W. de Wit, Formation of a cerium-based conversion coating on AA2024: relationship with the microstructure, Surface and Coatings Technology, 176 (2004) 365-381.
[16] W. Zhang, R.G. Buchheit, Hydrotalcite Coating Formation on Al-Cu-Mg Alloys from Oxidizing Bath Chemistries, CORROSION, 58 (2002) 591-600.
[17] B. Kuznetsov, M. Serdechnova, J. Tedim, M. Starykevich, S. Kallip, M.P. Oliveira, T. Hack, S. Nixon, M.G.S. Ferreira, M.L. Zheludkevich, Sealing of tartaric sulfuric (TSA) anodized AA2024 with nanostructured LDH layers, RSC Advances, 6 (2016) 13942-13952.

[18] F. Zhang, L. Zhao, H. Chen, S. Xu, D.G. Evans, X. Duan, Corrosion Resistance of Superhydrophobic Layered Double Hydroxide Films on Aluminum, Angewandte Chemie International Edition, 47 (2008) 2466-2469.
[19] J. Tedim, M.L. Zheludkevich, A.N. Salak, A. Lisenkov, M.G.S. Ferreira, Nanostructured LDH-container layer with active protection functionality, Journal of Materials Chemistry, 21 (2011) 15464-15470.
[20] U. Schubert, N. Huesing, A. Lorenz, Hybrid Inorganic-Organic Materials by Sol-Gel Processing of Organofunctional Metal Alkoxides, Chemistry of Materials, 7 (1995) 2010-2027.
[21] N.C. Rosero-Navarro, L. Paussa, F. Andreatta, Y. Castro, A. Durán, M. Aparicio, L. Fedrizzi, Optimization of hybrid sol–gel coatings by combination of layers with complementary properties for corrosion protection of AA2024, Progress in Organic Coatings, 69 (2010) 167-174.
[22] N.N. Voevodin, N.T. Grebasch, W.S. Soto, F.E. Arnold, M.S. Donley, Potentiodynamic evaluation of sol–gel coatings with inorganic inhibitors, Surface and Coatings Technology, 140 (2001) 24-28.
[23] K.A. Yasakau, S. Kallip, M.L. Zheludkevich, M.G.S. Ferreira, Active corrosion protection of AA2024 by sol–gel coatings with cerium molybdate nanowires, Electrochimica Acta, 112 (2013) 236-246.
[24] K.A. Yasakau, M.L. Zheludkevich, O.V. Karavai, M.G.S. Ferreira, Influence of inhibitor addition on the corrosion protection performance of sol–gel coatings on AA2024, Progress in Organic Coatings, 63 (2008) 352-361.
[25] Z. Tian, H. Shi, F. Liu, S. Xu, E.-H. Han, Inhibiting effect of 8-hydroxyquinoline on the corrosion of silane-based sol–gel coatings on AA 2024-T3, Progress in Organic Coatings, 82 (2015) 81-90.
[26] Y. Liang, M. Wang, C. Wang, J. Feng, J. Li, L. Wang, J. Fu, Facile Synthesis of Smart Nanocontainers as Key Components for Construction of Self-Healing Coating with Superhydrophobic Surfaces, Nanoscale Research Letters, 11 (2016) 231.
[27] D. Borisova, H. Möhwald, D.G. Shchukin, Mesoporous Silica Nanoparticles for Active Corrosion Protection, ACS Nano, 5 (2011) 1939-1946.
[28] C. Tao, F. JiaJun, An intelligent anticorrosion coating based on pH-responsive supramolecular nanocontainers, Nanotechnology, 23 (2012) 505705.
[29] K.A. Yasakau, J. Tedim, M.L. Zheludkevich, M.G.S. Ferreira, Active Corrosion Protection by Nanoparticles and Conversion Films of Layered Double Hydroxides, CORROSION, 70 (2014) 436-445.
[30] S.P.V. Mahajanam, R.G. Buchheit, Characterization of Inhibitor Release from Zn-Al-[V10O28]6− Hydrotalcite Pigments and Corrosion Protection from Hydrotalcite-Pigmented Epoxy Coatings, CORROSION, 64 (2008) 230-240.
[31] J. Tedim, M.L. Zheludkevich, A.C. Bastos, A.N. Salak, J. Carneiro, F. Maia, A.D. Lisenkov, A.B. Oliveira, M.G.S. Ferreira, Effect of Surface Treatment on the Performance of LDH Conversion Films, ECS Electrochemistry Letters, 3 (2014) C4-C8.
[32] A.N. Salak, J. Tedim, A.I. Kuznetsova, M.L. Zheludkevich, M.G.S. Ferreira, Anion exchange in Zn–Al layered double hydroxides: In situ X-ray diffraction study, Chemical Physics Letters, 495 (2010) 73-76.
[33] K.A. Yasakau, J. Carneiro, M.L. Zheludkevich, M.G.S. Ferreira, Influence of sol-gel process parameters on the protection properties of sol–gel coatings applied on AA2024, Surface and Coatings Technology, 246 (2014) 6-16.

[34] M.L. Zheludkevich, K.A. Yasakau, A.C. Bastos, O.V. Karavai, M.G.S. Ferreira, On the application of electrochemical impedance spectroscopy to study the self-healing properties of protective coatings, Electrochemistry Communications, 9 (2007) 2622-2628.
[35] M.E. Orazem, B. Tribollet, Time-Constant Dispersion, in: Electrochemical Impedance Spectroscopy, John Wiley & Sons, Inc., 2008, pp. 233-263.
[36] L. Paussa, N.C. Rosero-Navarro, F. Andreatta, Y. Castro, A. Duran, M. Aparicio, L. Fedrizzi, Inhibition effect of cerium in hybrid sol–gel films on aluminium alloy AA2024, Surface and Interface Analysis, 42 (2010) 299-305.
[37] M. Quinet, B. Neveu, V. Moutarlier, P. Audebert, L. Ricq, Corrosion protection of sol–gel coatings doped with an organic corrosion inhibitor: Chloranil, Progress in Organic Coatings, 58 (2007) 46-53.
[38] C.H. Hsu, F. Mansfeld, Technical Note: Concerning the Conversion of the Constant Phase Element Parameter Y0 into a Capacitance, CORROSION, 57 (2001) 747-748.
[39] G.J. Brug, A.L.G. van den Eeden, M. Sluyters-Rehbach, J.H. Sluyters, The analysis of electrode impedances complicated by the presence of a constant phase element, Journal of Electroanalytical Chemistry and Interfacial Electrochemistry, 176 (1984) 275-295.
[40] B. Hirschorn, M.E. Orazem, B. Tribollet, V. Vivier, I. Frateur, M. Musiani, Determination of effective capacitance and film thickness from constant-phase-element parameters, Electrochimica Acta, 55 (2010) 6218-6227.
[41] K.D. Ralston, S. Chrisanti, T.L. Young, R.G. Buchheit, Corrosion Inhibition of Aluminum Alloy 2024-T3 by Aqueous Vanadium Species, Journal of The Electrochemical Society, 155 (2008) C350-C359.
[42] S.H. Hussein Al Ali, M. Al-Qubaisi, M.Z. Hussein, M. Ismail, Z. Zainal, M.N. Hakim, Comparative study of Mg/Al- and Zn/Al-layered double hydroxide-perindopril erbumine nanocomposites for inhibition of angiotensin-converting enzyme, International Journal of Nanomedicine, 7 (2012) 4251-4262.
[43] H. Abdolmohammad-Zadeh, K. Nejati, E. Ghorbani, Synthesis, Characterization, and Application of Zn–Al Layered Double Hydroxide as a Nano-Sorbent for the Removal of Direct Red 16 from Industrial Wastewater Effluents, Chemical Engineering Communications, 202 (2015) 1349-1359.
[44] C. Carneiro, F. Oliveira, J. Nogueira, A. Mendes, Permeability of paint films towards chloride ion, JCT Research, 3 (2006) 159-162.
[45] O.C.G.A. G. K. van der Wel, Moisture transport and equilibrium in organic coatings, in, Delft University of Technology, 2000, pp. p. 125-152.
[46] O. Guseva, P. Schmutz, T. Suter, O. von Trzebiatowski, Modelling of anodic dissolution of pure aluminium in sodium chloride, Electrochimica Acta, 54 (2009) 4514-4524.
[47] M. Iannuzzi, G.S. Frankel, Mechanisms of corrosion inhibition of AA2024-T3 by vanadates, Corrosion Science, 49 (2007) 2371-2391.
[48] M. Iannuzzi, T. Young, G.S. Frankel, Aluminum Alloy Corrosion Inhibition by Vanadates, Journal of The Electrochemical Society, 153 (2006) B533-B541.
[49] M. Iannuzzi, J. Kovac, G.S. Frankel, A study of the mechanisms of corrosion inhibition of AA2024-T3 by vanadates using the split cell technique, Electrochimica Acta, 52 (2007) 4032-4042.
[50] K.D. Ralston, T.L. Young, R.G. Buchheit, Electrochemical Evaluation of Constituent Intermetallics in Aluminum Alloy 2024-T3 Exposed to Aqueous Vanadate Inhibitors, Journal of The Electrochemical Society, 156 (2009) C135-C146.

[51] J. C. F. Baes, and R. E. Mesme, The Hydrolysis of Cations, in: R. E. (Ed.), Krieger Publishing Company, Inc., Malabar, FL, 1986, pp. 512.
[52] E. McCafferty, The electrode kinetics of pit initiation on aluminum, Corrosion Science, 37 (1995) 481-492.
[53] S.i. Pyun, S.M. Moon, S.H. Ahn, S.S. Kim, Effects of Cl−, NO− 3 and SO2− 4 ions on anodic dissolution of pure aluminum in alkaline solution, Corrosion Science, 41 (1999) 653-667.
[54] S.-I. Pyun, S.-M. Moon, The inhibition mechanism of pitting corrosion of pure aluminum by nitrate and sulfate ions in neutral chloride solution, Journal of Solid State Electrochemistry, 3 (1999) 331-336.
[55] J. Tedim, A. Kuznetsova, A.N. Salak, F. Montemor, D. Snihirova, M. Pilz, M.L. Zheludkevich, M.G.S. Ferreira, Zn–Al layered double hydroxides as chloride nanotraps in active protective coatings, Corrosion Science, 55 (2012) 1-4.
[56] M. Iannuzzi, G.S. Frankel, Inhibition of Aluminum Alloy 2024 Corrosion by Vanadates: An In Situ Atomic Force Microscopy Scratching Investigation, CORROSION, 63 (2007) 672-688.
[57] J. Li, B. Hurley, R. Buchheit, Inhibition Performance Study of Vanadate on AA2024-T3 at High Temperature by SEM, FIB, Raman and XPS, Journal of The Electrochemical Society, 162 (2015) C219-C227.

Figure captions

Figure 1. A scheme of LDH synthesis and Sol-gel coating application.

Figure 2. SEM images of AA2024 surface after pre-treatments #1 (a) and #2 (b), and sol-gel coatings atop LDH(NO3) (c,d) and LDH(V2O7) (e,r) conversion layers on 2-steps pre-treated AA2024 (c,e) and 3-steps pre-treated (d,f) AA2024; a blank sol-gel coating (g); EDS spectra of sol-gel coated LDH(NO3) and LDH(V2O7) samples (h).

Figure 3. SEM micrographs (a,f) and EDS elemental maps of LDH(NO3) (a,b,c,d,e) and LDH(V2O7) (f,g,h,i,j) samples cross-sections before immersion.

Figure 4. EIS spectra of Control, #1LDH(NO3) and #1LDH(V2O7) coatings (a,b) and #2LDH(NO3) and #2LDH(V2O7) coatings (c,d) after 1 day (a,c) or 14 (b,d) days immersion in 0.5M NaCl solution; solid lines present EIS spectra fitting.

Figure 5. Equivalent circuits employed for fitting impedance spectra of Sol-gel coated system (a) and LDH/sol-gel coated systems (b).

Figure 6. Evolution of fitting parameters of EIS spectra during immersion. Graphs represent sol-gel coating resistance R_{coat} a), mixed oxide film resistance R_{mixed} b), oxide layer resistance R_{ox} c), capacitance C_{ox} d), and charge transfer resistance R_{ct} e).

Figure 7. SVET ionic currents maps measured on Control, #2LDH(NO3) and #2LDH(V2O7) sample during different times in 0.05 M NaCl.

Figure 8. SEM images of sol-gel coatings after immersion tests #1LDH(NO3) a), #2LDH(NO3) c), and #1LDH(V2O7) b) and #2LDH(V2O7) d); EDS spectra (e) acquired at LDH islands #2LDH(NO3) and #2LDH(V2O7) samples.

Figure 9. GDOES elemental profiles obtained on #2LDH(NO3) (a,b) and #2LDH(V2O7) (c,d) samples before (a,c) and after (b,d) EIS tests (approximately 1 month of immersion in 0.5 M NaCl).

Figure 10. Release profiles of vanadate (VO3) species. Error bars correspond to standard deviation and lines are obtained by adjacent -averaging method for guidance purposes.

Figure 11. Mechanism of inhibition of AA2024 by a sol-gel/LDH(V2O7) protective coating; and SEM/EDS analysis of a coating containing LDH(V2O7) layer showing buried S-

phase intermetallic and defined signals of Al, Cu and Mg on the EDS graph acquired at the intermetallic.

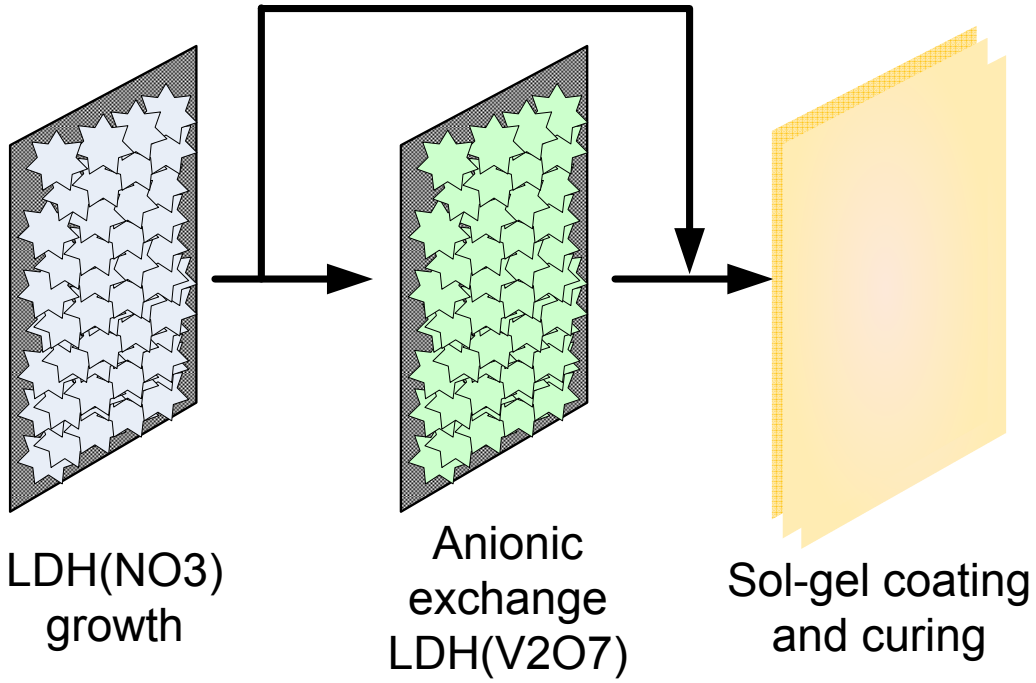

Figure 1. A scheme of LDH synthesis and Sol-gel coating application.

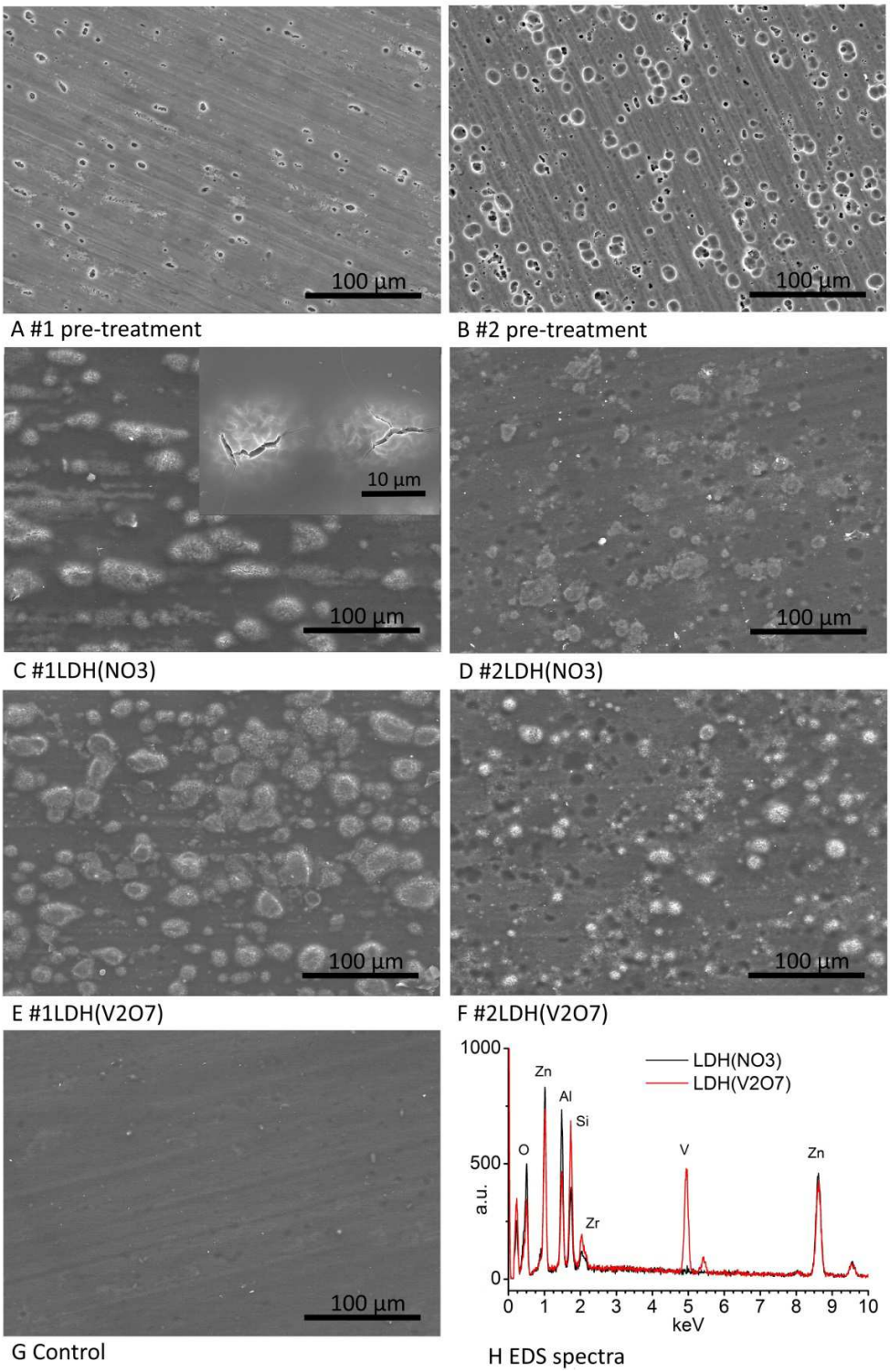

Figure 2. SEM images of AA2024 surface after pre-treatments #1 (a) and #2 (b), and sol-gel coatings atop LDH(NO3) (c,d) and LDH(V2O7) (e,r) conversion layers on 2-steps pre-treated AA2024 (c,e) and 3-steps pre-treated (d,f) AA2024; a blank sol-gel coating (g); EDS spectra of sol-gel coated LDH(NO3) and LDH(V2O7) samples (h).

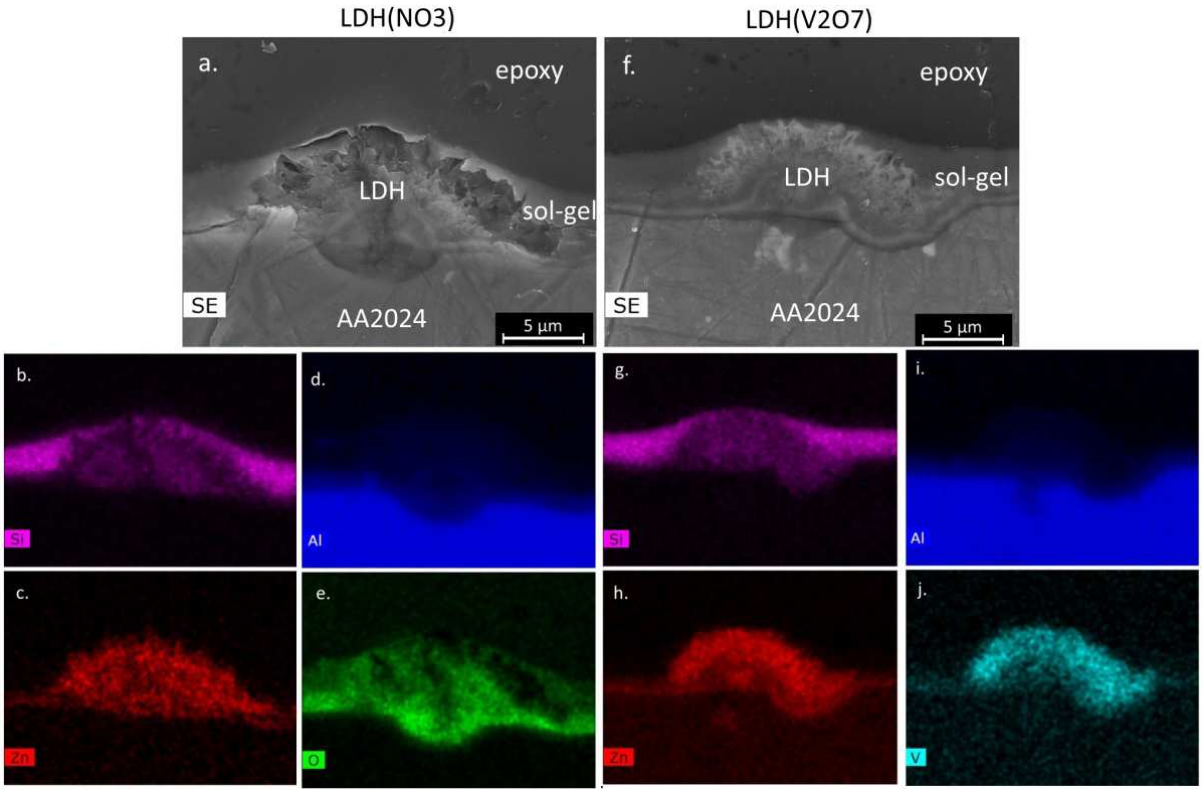

Figure 3. SEM micrographs (a,f) and EDS elemental maps of LDH(NO3) (a,b,c,d,e) and LDH(V2O7) (f,g,h,i,j) samples cross-sections before immersion.

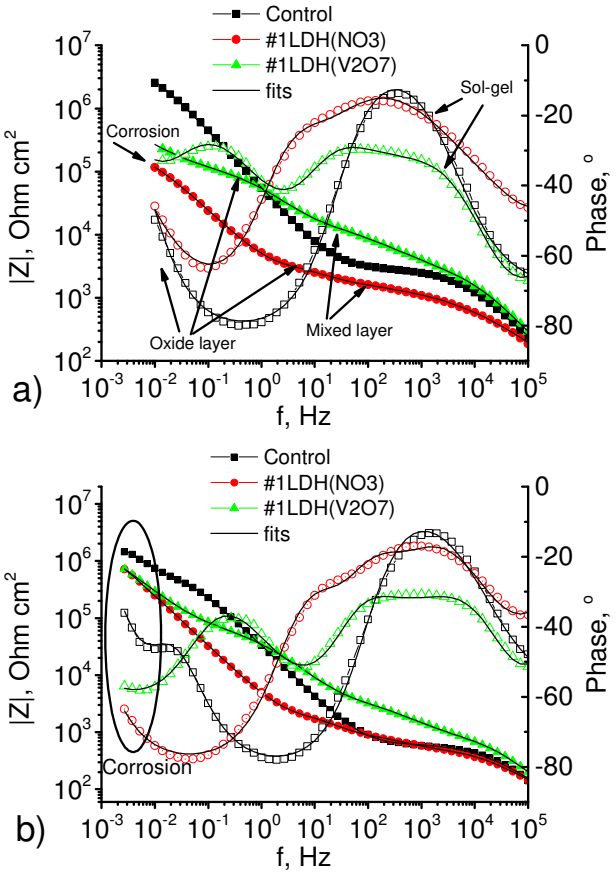
Control
#1LDH(NO3)
#1LDH(V2O7)
fits
Sol-gel
Corrosion
Oxide layer
Mixed layer
|Z|, Ohm cm2
Phase, °
f, Hz
a)
b)

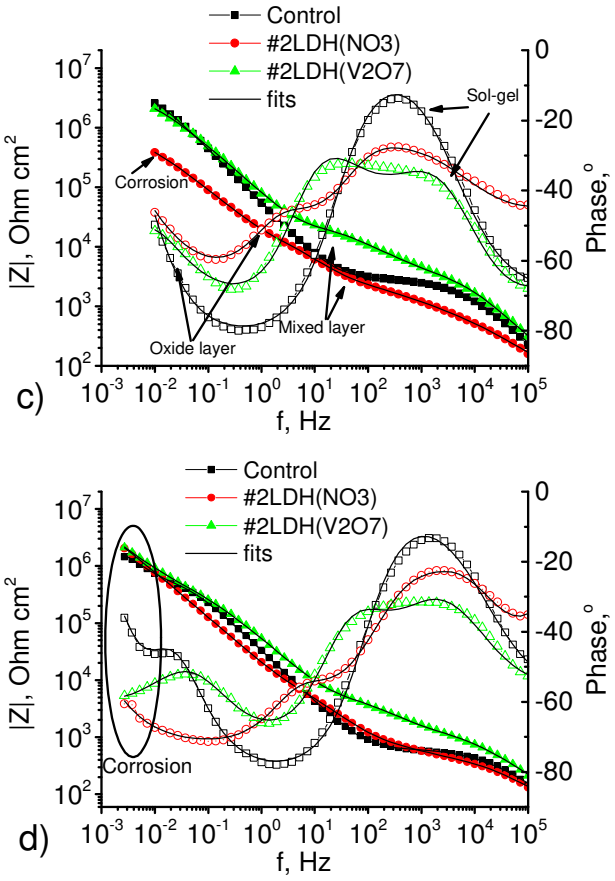

Figure 4. EIS spectra of Control, #1LDH(NO3) and #1LDH(V2O7) coatings (a,b) and #2LDH(NO3) and #2LDH(V2O7) coatings (c,d) after 1 day (a,c) or 14 (b,d) days immersion in 0.5M NaCl solution; solid lines present EIS spectra fitting.

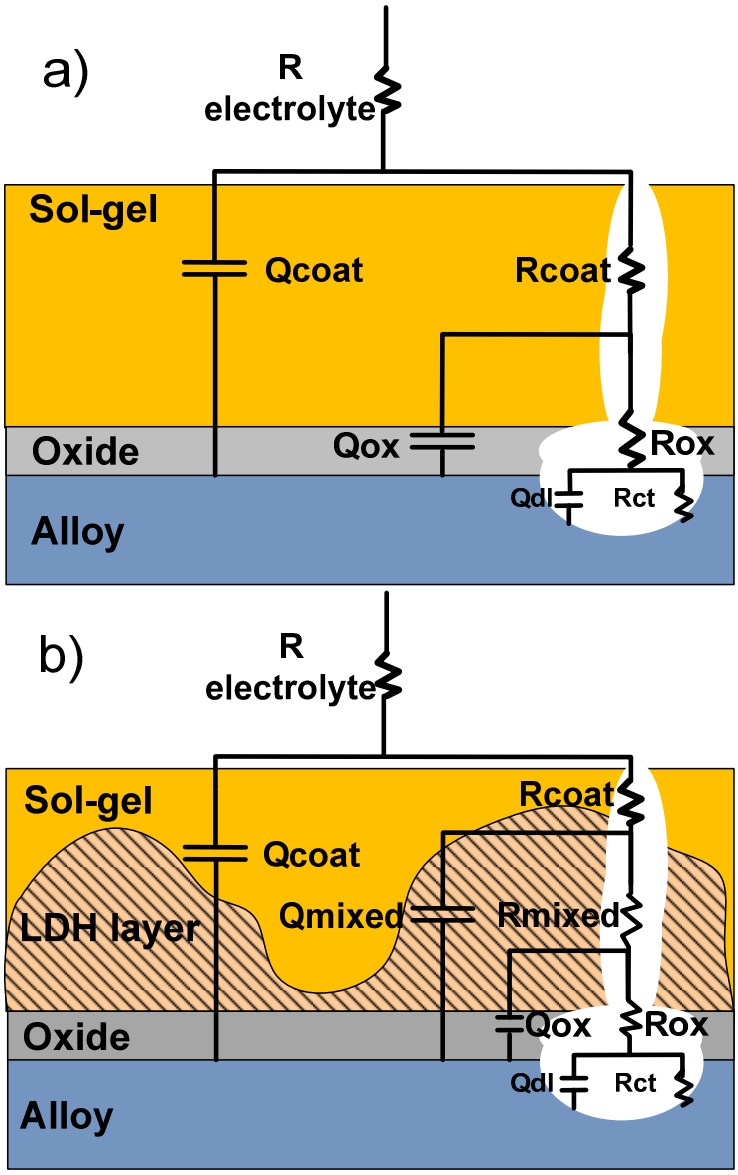

Figure 5. Equivalent circuits employed for fitting impedance spectra of Sol-gel coated system (a) and LDH/sol-gel coated systems (b).

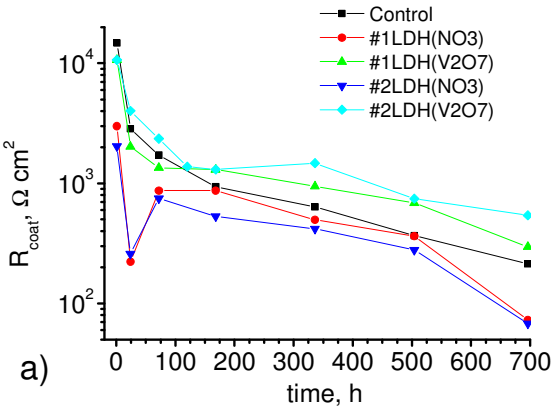
Control
#1LDH(NO3)
#1LDH(V2O7)
#2LDH(NO3)
#2LDH(V2O7)
R_{coat}, Ω cm^2
10^4
10^3
10^2
0 100 200 300 400 500 600 700
time, h
a)

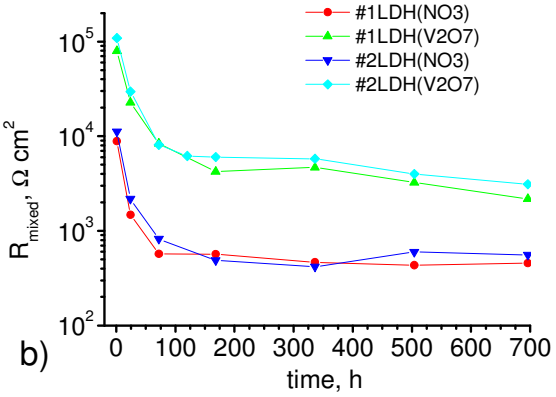
#1LDH(NO3)
#1LDH(V2O7)
#2LDH(NO3)
#2LDH(V2O7)
R_{mixed}, Ω cm^2
10^5
10^4
10^3
10^2
0 100 200 300 400 500 600 700
time, h
b)

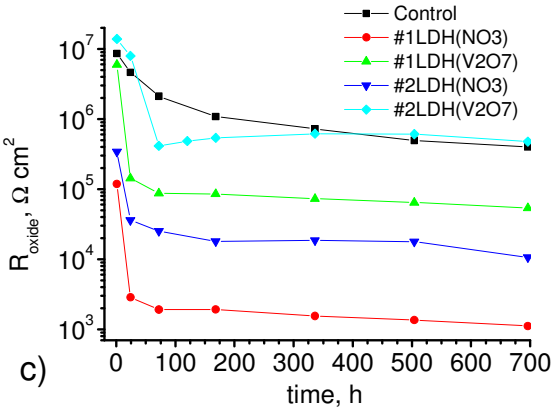
Control
#1LDH(NO3)
#1LDH(V2O7)
#2LDH(NO3)
#2LDH(V2O7)
R_{oxide}, Ω cm^2
10^7
10^6
10^5
10^4
10^3
0 100 200 300 400 500 600 700
time, h
c)

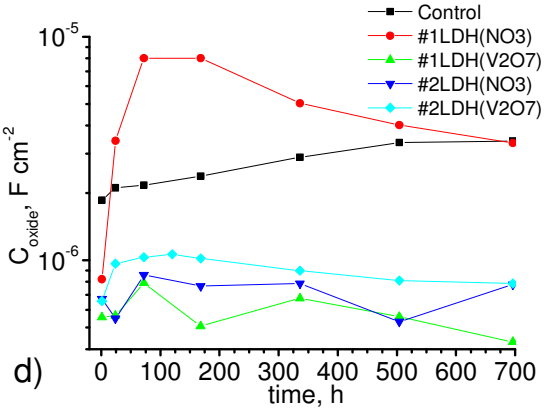
Control
#1LDH(NO3)
#1LDH(V2O7)
#2LDH(NO3)
#2LDH(V2O7)
C_{oxide}, F cm^{-2}
10^{-5}
10^{-6}
0 100 200 300 400 500 600 700
time, h
d)

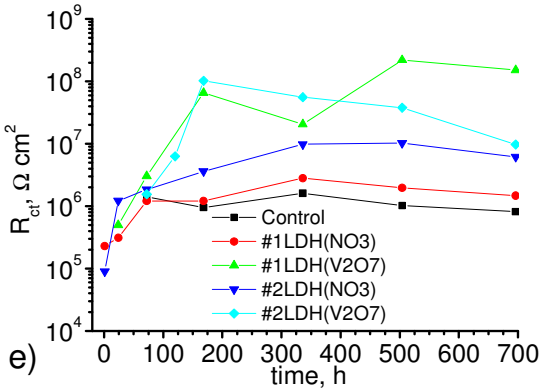

Figure 6. Evolution of fitting parameters of EIS spectra during immersion. Graphs represent sol-gel coating resistance R_{coat} a), mixed oxide film resistance R_{mixed} b), oxide layer resistance R_{ox} c), capacitance C_{ox} d), and charge transfer resistance R_{ct} e).

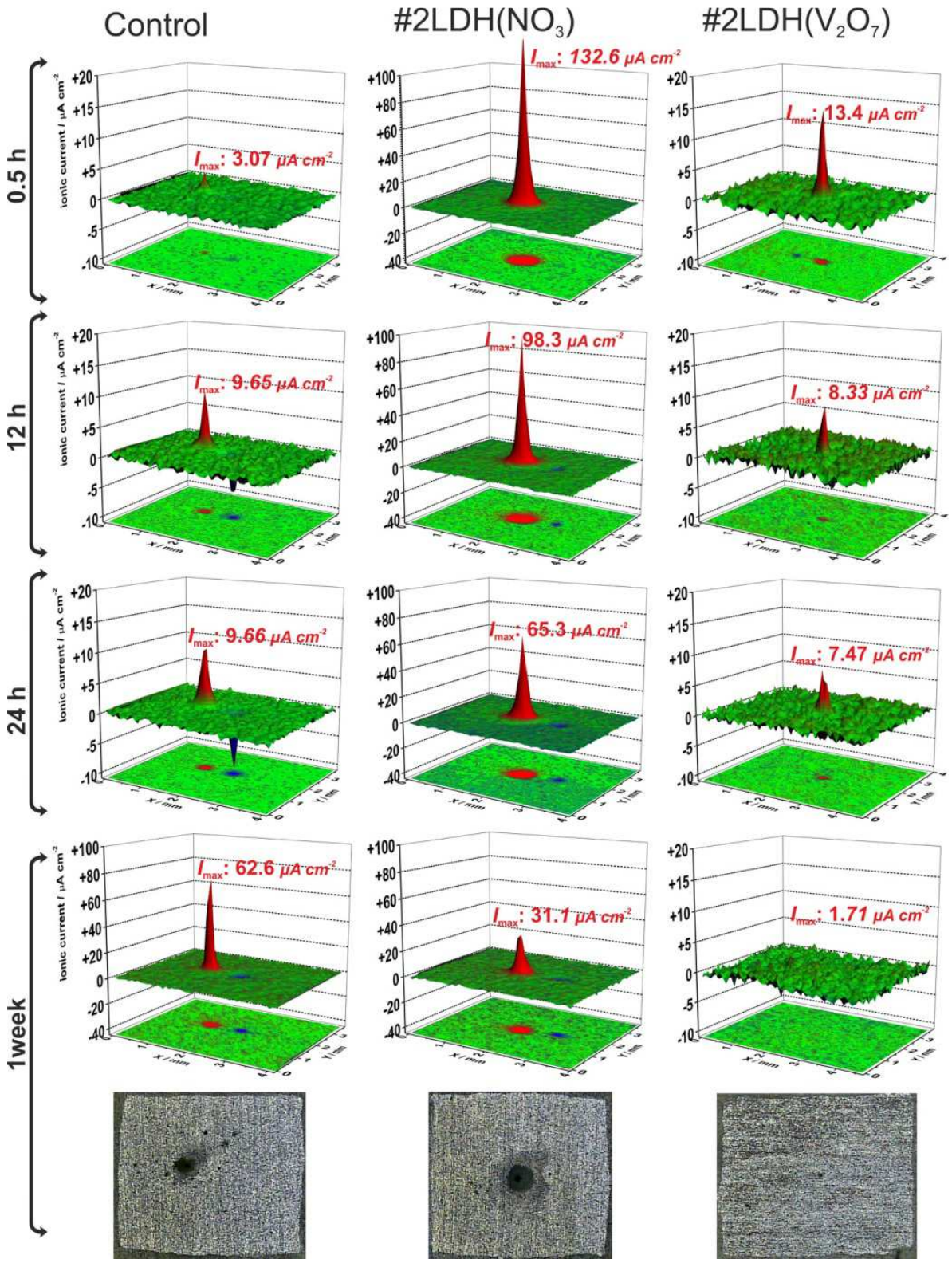

Figure 7. SVET ionic currents maps measured on Control, #2LDH(NO3) and #2LDH(V2O7) sample during different times in 0.05 M NaCl.

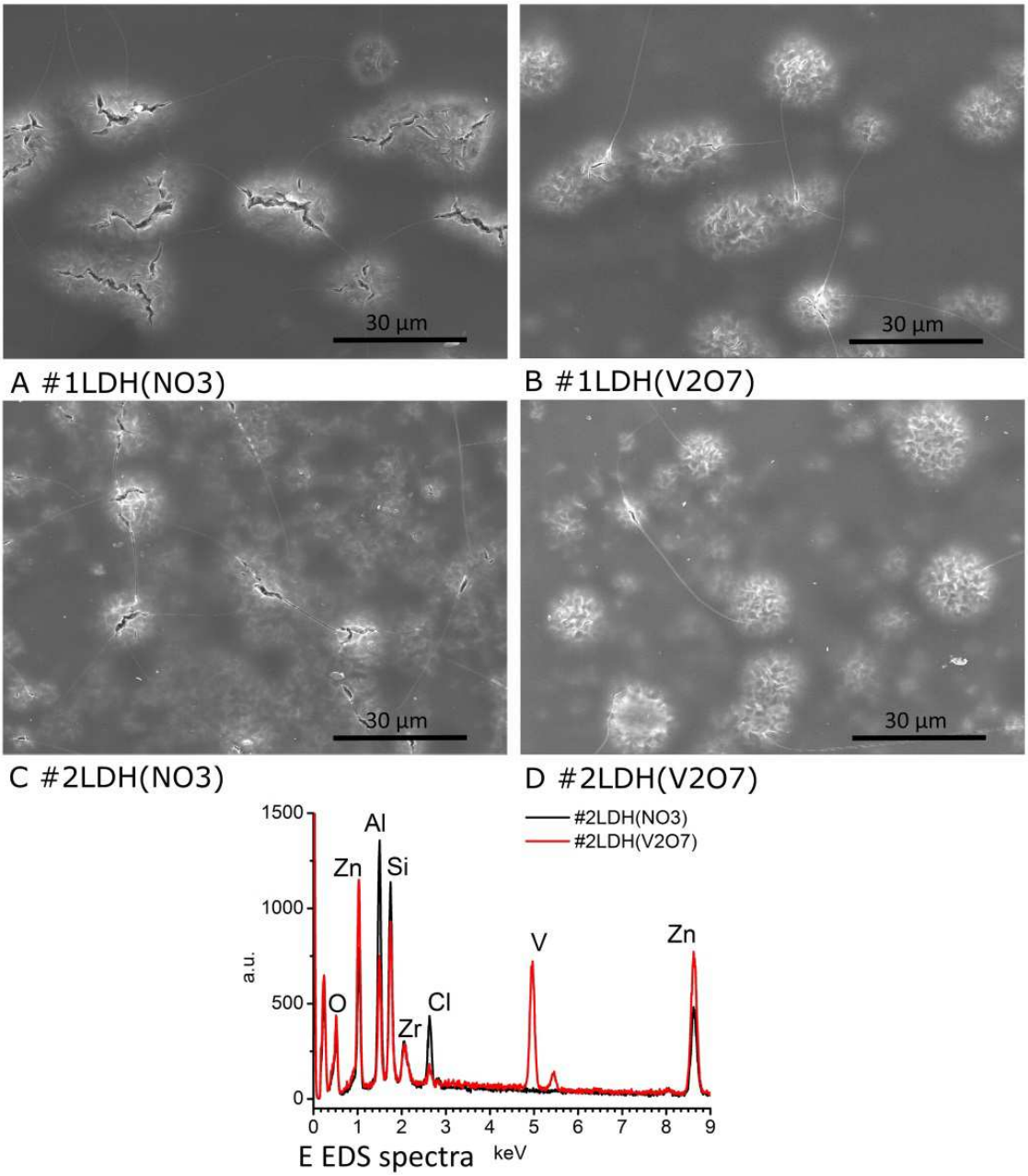

Figure 8. SEM images of sol-gel coatings after immersion tests #1LDH(NO3) a), #2LDH(NO3) c), and #1LDH(V2O7) b) and #2LDH(V2O7) d); EDS spectra (e) acquired at LDH islands #2LDH(NO3) and #2LDH(V2O7) samples.

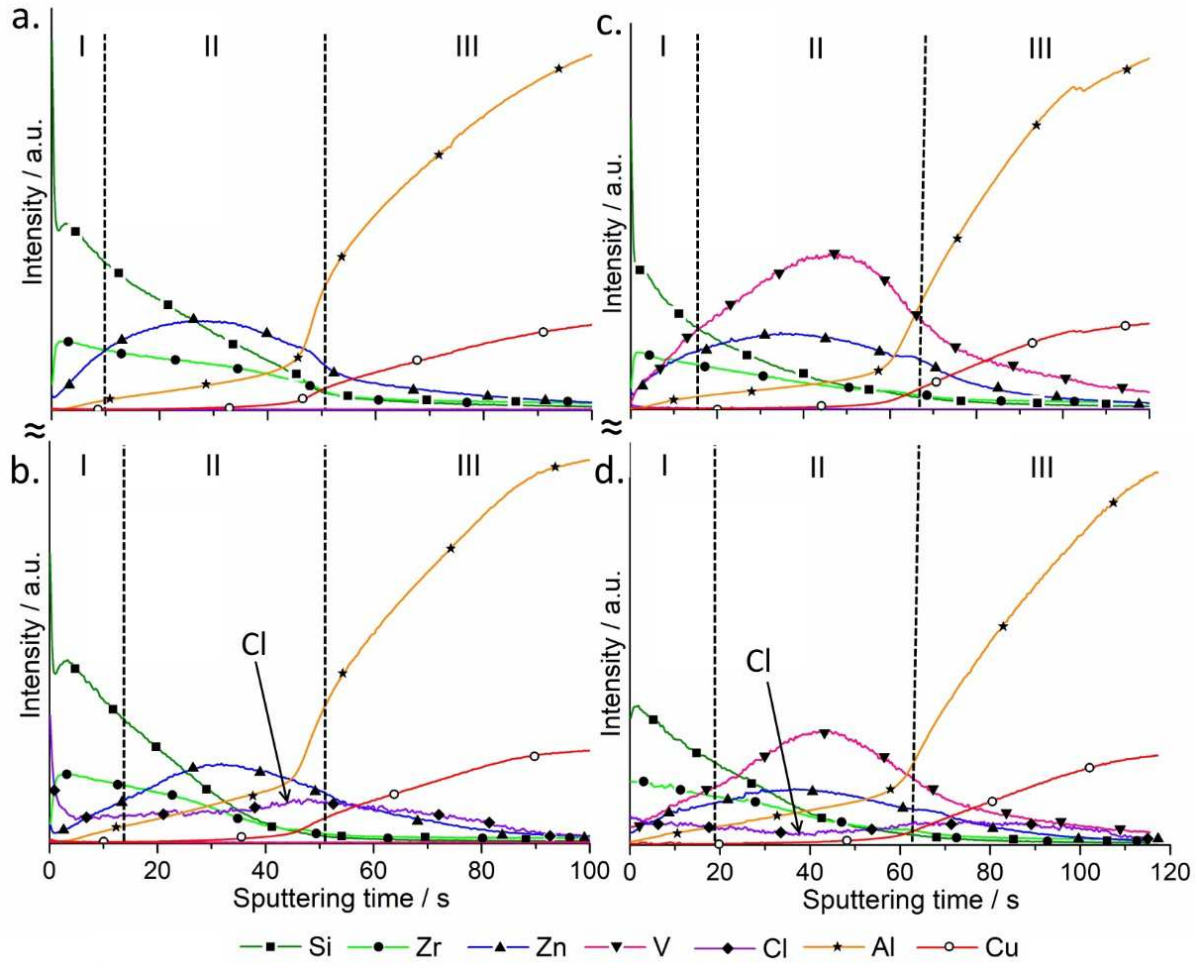

Figure 9. GDOES elemental profiles obtained on #2LDH(NO3) (a,b) and #2LDH(V2O7) (c,d) samples before (a,c) and after (b,d) EIS tests (approximately 1 month of immersion in 0.5 M NaCl).

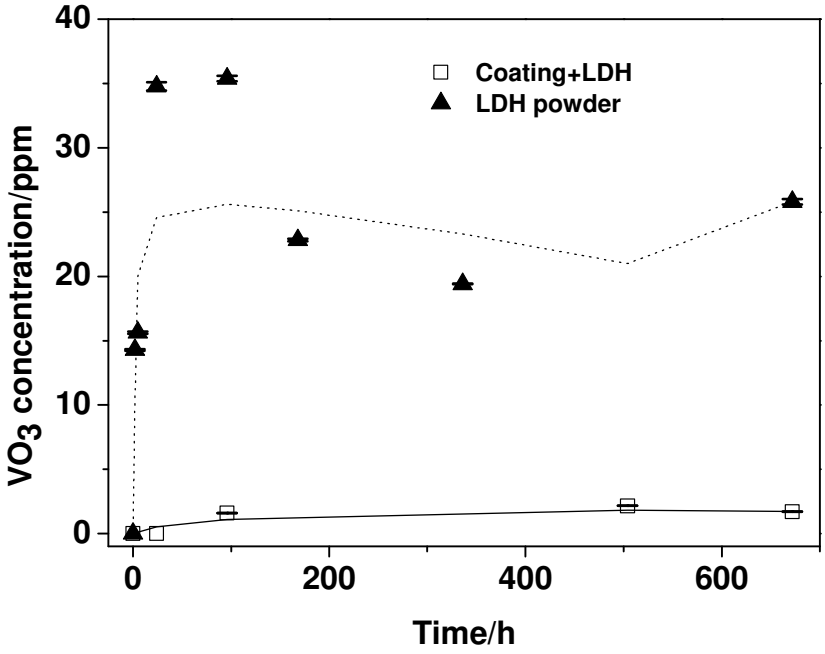

Figure 10. Release profiles of vanadate (VO_3) species. Error bars correspond to standard deviation and lines are obtained by adjacent -averaging method for guidance purposes.

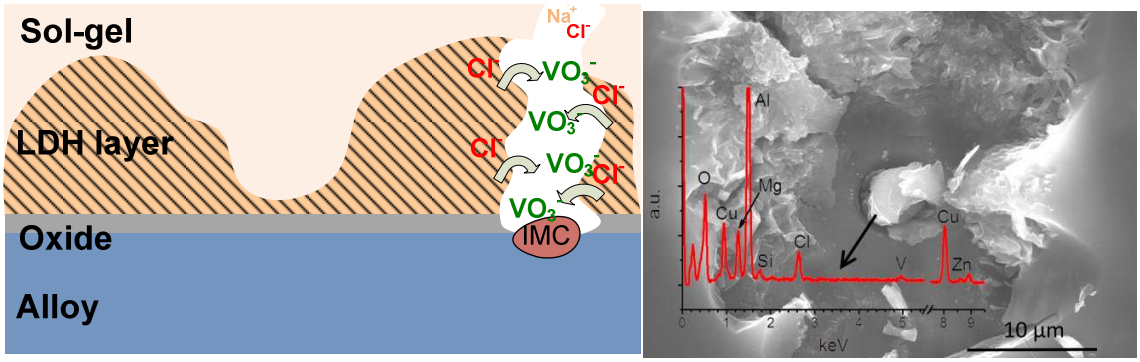

Figure 11. Mechanism of inhibition of AA2024 by a sol-gel/LDH(V2O7) protective coating; and SEM/EDS analysis of a coating containing LDH(V2O7) layer showing buried S-phase intermetallic and defined signals of Al, Cu and Mg on the EDS graph acquired at the intermetallic.